Heliyon 9 (2023) e22090

Contents lists available at ScienceDirect

Heliyon

journal homepage: www.cell.com/heliyon

Suppresses of LIM kinase 2 promotes radiosensitivity in radioresistant non-small cell lung cancer cells

Chao Tian [a,1], Zhen Peng [a,1], Lei Chang [b,1], Xinzhou Deng [a], Shan Jiang [a], Jiahui Han [c], Can Ye [a], Yutao Yan [a,*], Zhiguo Luo [a,**]

[a] Department of Clinical Oncology, Hubei Clinical Research Center for Precise Diagnosis and Treatment of Liver Cancer, Taihe Hospital, Hubei University of Medicine, Shiyan, China
[b] Department of Urology, Central Hospital of Wuhan, Tongji Medical College, Huazhong University of Science and Technology, Wuhan, 430014, China
[c] Department of Clinical Oncology, Taihe Hospital, Jinzhou Medical University Union Training Base, Shiyan, Hubei, 442000, China

ARTICLE INFO

Keywords:
LIMK2
Radiation resistance
NSCLC
Migration
Clone formation

ABSTRACT

Radiation resistance has always been one of the main obstacles to tumor radiotherapy. Therefore, understanding the mechanisms underlying radiotherapy resistance is a focus of research. In this study, we induced two radiation-resistant cell lines to mimic the radiation resistance of NSCLC and investigated the mechanisms of radiotherapy resistance. Cell radiosensitivity was analyzed by single-cell gel electrophoresis, colony formation and tumor sphere formation assays. A wound healing assay was used to analyze cell migration. Western blotting and siRNA were used to identify the potential mechanism. In animal model experiments, xenograft tumors were used to verify the difference between radiotherapy-resistant and nonresistant NSCLC models after radiotherapy. Our results showed that NSCLC radiation-resistant cells exhibited more radioresistance and migratory abilities under low-dose irradiation. The expression of LIMK2 and p-CFL1 were upregulated in NSCLC radiation-resistant cells. Knockdown of LIMK2 significantly enhanced the radiosensitivity of NSCLC-resistant cells. In vivo, low-dose radiotherapy suppressed tumor growth, induced apoptosis and upregulated the expression of LIMK2 in xenograft tumors. However, radiotherapy had little effect on the NSCLC radiation resistance model. In conclusion, NSCLC radiation-resistant cells exhibit more radioresistance and migratory ability under low-dose irradiation. Strikingly, knockdown of LIMK2 enhanced the radiosensitivity of NSCLC-resistant cells.

1. Introduction

Lung cancer is one of the most lethal tumors in the world. The most dominant type is non-small cell lung cancer (NSCLC) [1]. The treatments for NSCLC include surgery, radiation therapy (RT), chemotherapy, immunotherapy, targeted therapy, or a combined modality approach [2]. Surgical resection remains the primary and preferred approach to the treatment of stage I and II NSCLC. The

Abbreviations: NSCLC, non-small cell lung cancer; LIMK2, LIM kinase 2.

* Corresponding author.
** Corresponding author.
E-mail addresses: yanyutao_111@163.com (Y. Yan), Luozhiguo@hbmu.edu.cn (Z. Luo).

[1] Equal contributors.

https://doi.org/10.1016/j.heliyon.2023.e22090
Received 24 August 2023; Received in revised form 31 October 2023; Accepted 3 November 2023
Available online 8 November 2023

use of adjuvant chemotherapy for stage II NSCLC is recommended and has shown benefit. The use of adjuvant radiation or chemotherapy for stage I NSCLC is of unproven benefit. RT is used to relieve symptoms and improve the quality of life of patients with advanced NSCLC. In combination with chemotherapy or immunotherapy, it enhances treatment efficacy and improves patient outcomes [3]. The main mechanism of radiotherapy is inflicting direct DNA damage, including DNA single-strand breaks (SSBs) and double-strand breaks (DSBs), which kills tumor cells [4,5].

Although radiation is generally an effective tool for cancer treatment, resistance often results in treatment failure [6]. It has been demonstrated that the radioresistance mechanisms include an altered cell cycle, repopulation by tumor stem cells, evasion of apoptosis, altered DNA damage response (DDR) and enhanced DNA repair [7,8]. To overcome radioresistance, more combination methods are being used for tumor treatment; unfortunately, this produces more side effects [9]. Therefore, it is necessary to study the mechanism and treatment strategies of radiotherapy resistance further.

LIM kinase (LIMK) is a serine/threonine-protein kinase that includes LIMK1 and LIMK2 members. It is an upstream protein that regulates Cofilin and catalyzes Cofilin phosphorylation [10]. LIMK2 can protect cells from death and promote cancer cell proliferation and chemotherapeutic resistance [11,12]. It plays a critical role in regulating actin dynamics by phosphorylating cofilin, and it is associated with cancer metastasis, migration, angiogenesis and invasion. Cofilin-1 (CFL1) is involved in regulation of the actin cytoskeleton in response to various extracellular signals, such as growth factors, hormones, and cytokines. Aberrant expression or dysfunction of CFL1 has been implicated in several human diseases, including cancer, Alzheimer's disease, and heart disease. Dysregulation of the LIMK2-CFL1 pathway has been implicated in various human diseases, such as cancer and neurodegenerative disorders [13]. Membrane skeleton proteins act as an important role in promoting tumor cell migration and invasion [14]. During our experiment, we observed that radio-resistant cells exhibited greater migration ability following X-ray irradiation compared to parent cells. According to previous studies, LIMK2 has been shown to play a role in tumor proliferation and metastasis [15]. Therefore, it was inferred that cytoskeletal proteins may be crucial for radiotherapy resistance of the radio-resistant strains.

In this study, we focused on the pivotal role of LIMK2 on the radioresistance of NSCLC. By inducing a radiation-resistant NSCLC cell model, we demonstrated that the expression of LIMK2 was upregulated in radioresistant NSCLC cell lines and tumors. Downregulation of LIMK2 expression can enhance the sensitivity of NSCLC-resistant cells to radiotherapy, including cell proliferation, colony formation and cell migration suppression, which indicated LIMK2 may be a potential target for the prevention and treatment of radioresistance in NSCLC.

2. Materials and methods

2.1. Ethics

All of the animal experiments were performed in accordance with the guidelines and animal use regulations of the Hubei University of Medicine and were approved by the Institutional Animal Care and Use Committee (IACUC) of the Hubei University of Medicine (Hubei University of Medicine -No.2021–067). This study conformed to the NIH Guide for the Care and Use of Laboratory Animals (NIH publication no. 85–23, revised 2011). Reporting of the procedures and results followed the Animal Research: Reporting of In Vivo Experiments (ARRIVE) guidelines.

2.2. Cell cultures and treatment

A549, H1299, A549R and H1299R cells were cultured in DMEM (GE Healthcare Life Sciences HyClone Laboratories, Utah) supplemented with 10 % (v/v) fetal bovine serum (FBS) and 1 % penicillin–streptomycin at 37 °C with 5 % CO_2.

NSCLC radioresistance cell lines (A549R, H1299R) were induced by X-ray exposure of the NSCLC parental cell lines (A549, H1299) in our laboratory. A549 and H1299 cells were exposed to fractionated X-ray radiation (2–3 times/week, 2 Gy/time, with a total dose of 80 Gy) by a linear accelerator (X-RAD 320, Precision X-rays Inc., North Branford, CT, USA). Cells were cultured in a T25 culture flask with 5 mL medium, and half of the medium was changed after each irradiation session. The radioresistant cells were used after completion of induction. At present, there is no specific molecular marker as the standard for the detection of radiation resistance cells. Cloning and comet experiments are usually used as the gold standard for the detection of radiation sensitivity [16,17].

2.3. Main antibodies and reagents

Counting kit-8 (CCK-8, Dojindo Laboratories, Japan), Annexin V-FITC kit (88-8005-72; eBioscience Inc., San Diego, CA, USA), DAPI (BL150A, Biosharp, China), EGF (AF-100-15) and bFGF (100-18 B) were purchased from Peprotech (USA). B27 (12,587–010, Gibco, USA), rabbit anti-LIMK2 (A5409), rabbit anti-p-CFL1 (AP0178), rabbit anti-CFL1 (A1704) and rabbit anti-N-cadherin (A19083) were purchased from ABclonal (Abclonal Technology Co., Ltd., China). Rabbit anti-p-BCL2 (2827) and BCL2 (4223) were purchased from CST (Cell Signaling Technology, Inc., USA) and a Ribo Transfection kit (C10511-05) was purchased from RibioBio Co., Ltd.

2.4. Single-cell gel electrophoresis (comet assay)

A549, H1299, A549R and H1299R cells were irradiated with 0, 2 or 4 Gy before performing comet assays. The comet assays were performed according to international standard guidelines with slight modifications [18]. In brief, cells (10^4/10 μL) were lysed at 4 °C for 30 min. We use the alkaline lysate, so we detect all DNA damage including single and double strand breaks. After lysis, alkaline

enzymolysis and electrophoresis, the DNA was stained with DAPI (25 μg/mL, 20 μL) for 15 min protected from light. Then observe under a fluorescence microscope.

2.5. Cell migration experiment

A549, H1299, A549R and H1299R cells treated with 0, 2 or 4 Gy were collected and plated in 6-well plates to achieve 100 % confluence after 24 h. The cells were detached from the tissue culture plate and prepared as a single-cell suspension in culture media. The appropriate number of cells ($0.5–1 \times 10^6$) were plated in 6-well plates to achieve 100 % confluence in 24 h. Then, vertical wounds through the cells were made with a 10 μL pipette tip under a sterile environment. Cells were cultured in serum-free DMEM and maintained in an incubator at 37 °C with 5 % CO_2 [19]. The wound closure areas were recorded every 24 h and analyzed using ImageJ software (freely available at http://rsb.info.nih.gov/ij/).

2.6. Colony formation assay

A549, H1299, A549R and H1299R cells were irradiated with 0, 2 or 4 Gy and subjected to a colony formation assay according to the international standard guidelines with slight modifications [16]. In brief, cells were cultured in 6-well plates at a concentration of $1–2 \times 10^3$ cells/well, and fresh medium was added every 4 days. The culture was terminated at Day 14 when colonies were visible in the 6-well plates. After fixation with 4 % paraformaldehyde for 30 min, the cells were stained with 1 % (w/v) crystal violet for 30 min, and the dye solution was recycled. The colonies were counted directly by eye. Colony efficiency = (amount of colonies/number of seeded cells) × 100 %.

2.7. Tumor-sphere formation assay

A549, H1299, A549R and H1299R cells were irradiated with 0, 2 or 4 Gy and subjected to a tumor-sphere formation assay. The procedure was performed according to international standard guidelines with slight modifications [20]. In brief, $0.5–1 \times 10^3$ cells were cultured in 6-well plates (ultralow adsorption cell culture plates) with serum-free suspension medium (SFM). The culture was terminated on Day 10 when visible cell spheres were observed in the 6-well plates. SFM: DMEM/F12 basic medium +1× glutamine +1 × pyruvate +20 ng/mL EGF +10 ng/ml bFGF +2 % B27 (V/V). The cell spheres were counted under an optical microscope. Sphere formation efficiency (SFE) = number of cell spheres with a diameter greater than 75 μm per well/total number of originally seeded cells per well.

2.8. Cell viability assay

After irradiation and culture in 96-well plates with 5×10^3 cells per well, A549, H1299, A549R, and H1299R cells were subjected to a CCK8 assay to measure cell viability after 24 h. Specifically, the CCK8 reagent (10 μL) was incubated with the cells for 30 min, and the resulting absorbance was measured at 450 nm using an enzyme-linked immunosorbent assay reader.

2.9. Apoptosis assessment

The cells underwent X-ray irradiation at two different doses (0 and 4 Gy) and were subsequently cultured for 24 h. Afterward, the cells were harvested and labeled with FITC-Annexin V. Following a 15-min incubation at room temperature protected from light, the cells were analyzed within 1 h using flow cytometry (Beckman Coulter Quanta SC System). Data was analyzed by FlowJo_10.

2.10. RNA sequencing

A549 and A549R cells were collected to prepare for RNA sequencing. Total RNA was extracted and purified using an miR NeasyMini Kit (Qiagen) and checked for an RNA integrity number to inspect RNA integration by an RNA Nano 6000 Assay Kit of the Bioanalyzer2100 system (Agilent Technologies, CA, USA). The samples were clustered and sequenced by an Illumina platform from Metware Company Limited (Wuhan, China) and 150 bp paired-end reads were generated.

We used fastp to filter the original data, mainly to remove reads with adapters; when the N content in any sequencing reads exceeds 10 % of the base number of the reads, remove the paired reads; when any sequencing reads When the number of low-quality ($Q \leq 20$) bases contained in reads exceeds 50 % of the bases of the reads, this paired reads were removed. All subsequent analyses were based on clean reads. We downloaded the reference genome and its annotation files from the designated websites, and used HISAT to construct the index, and compare clean reads to the reference genome. The enrichment analysis was performed based on the hypergeometric test. For KEGG (Kyoto Encyclopedia of Genes and Genomes), the hypergeometric distribution test was performed with the unit of pathway; for GO (gene ontology) , it was performed based on the GO term. We used feature counts to calculate the gene alignment, and then calculated the FPKM of each gene based on the gene length. FPKM is currently the most commonly used method to estimate gene expression levels.

2.11. Immunofluorescence

A549 and A549R cells were fixed with 4 % paraformaldehyde for 20 min at room temperature, and treated with PBS containing 0.5 % Triton X-100 for 20 min at room temperature. Cells were then incubated with fluorescence labeling phalloidin 488 (Lablead, Beijing, China). The subsequent counterstained for nuclei was DAPI. All the Images were acquired with an Olympus FV3000RS fluorescence microscope system.

2.12. Western blot analysis

Cells were harvested and lysed in lysis buffer 30 min (RIPA + 0.5 mM PMSF + Protease Inhibitor Cocktail + Phosphatase Inhibitor Cocktail, absin, A Biochemical Company from China). The lysate was quantified with BCA kit, then mixed 5 × SDS loading buffer and boiled for 10 min. The 40 μg total cellular proteins of each group was electrophoresed on SDS-polyacrylamide gels and transferred by electroblotting onto a polyvinylidene fluoride (PVDF) membrane. The membrane was incubated with primary antibody after blocking with 5 % (w/v) BSA. The following primary antibodies were used: rabbit anti-LIMK2, p-CFL1, CFL1, N-cadherin, p-BCL2 and BCL2 antibody (1:1000, 4 °C, overnight). The membranes were then incubated with horseradish peroxidase-conjugated secondary antibodies (1:5000; Abcam, room temperature, 1 h). One hour later, the membranes were washed 3 times with TBST and then ECL luminescence reagent was used to detect the western blotting (MAO186-1, meilunbio, China). The β-tublin and β-actin were used as a loading control (1:5000, abclonal).

2.13. siRNA transfection

Cells were transfected with LIMK2 siRNA (50 nM) using a Ribo Transfection kit according to the manufacturer's instructions. S1, h-LIMK2 (GCTATTCACAGCAGATCTT; S2, h-LIMK2 CACGGCTCATAGTGGAAGA, Guangzhou Ribobio CO., LTD), and StealthTM RNAi negative controls (designated siNEG, TTCTCCGAGCGTCACGT) were purchased from Ribo Biotec.

2.14. NSCLC xenograft xenograft model

Male nude mice were obtained from the Hunan Laboratory Animal Center (China) and maintained under specific pathogen-free conditions. All of the experiments were performed in accordance with the guidelines and animal use regulations of the Hubei University of Medicine and approved by the Institutional Animal Care and Use Committee (IACUC) of the Hubei University of Medicine.

To minimize animal pain and suffering and ensure ethical treatment of the animals involved in this study, humane endpoints have been established. These endpoints include predetermined criteria for removing animals from the study in order to prevent unnecessary suffering. The humane endpoints in this study include the presence of behavioral abnormalities such as mania, changes in physical conditions such as abnormal eating or excretion, excessive tumor growth or the development of other health problems, or completion of a predetermined period of the study.

A total of 1×10^7/100 μL A549 or A549R cells were collected and mixed with equal volume matrix glue. Cell suspension (100 μL) was injected into the subcutaneous flanks of 4-week-old male nude mice (22–24 g). After 10 days, the mice bearing tumors were randomized and assigned to the control and irradiation groups (each group, n = 5). The weight of the mice and tumor volumes were determined every 2 days using the following equation: tumor volume (mm^3) = ½ × (tumor length) × (tumor width)^2. At the end of the experiment, mice were killed by excessive anesthesia with barbiturates, and the tumors were excised and measured, and then each tumor was fixed in 4 % paraformaldehyde for subsequent experiments.

2.15. TUNEL assay

Paraffin sections were studied by terminal deoxynucleotidyl transferase-mediated dUTP nick-end-labeling (TUNEL) assays. Staining was carried out according to the protocol provided by the supplier. Apoptosis was evaluated by counting the positive cells as well as the total number of cells in 10 arbitrarily selected fields at 400 × magnification in a blinded manner. We directly counted the number of positive cells in 5 random fields under a 20x microscope and then took the average as the number of positive cells for that slide.

2.16. Immunohistochemistry (IHC)

Paraffin sections were dewaxed with xylene and rehydrated with successive baths of ethanol (100 % × 2, 95 %, 90 %, 85 %, distilled water, 5 min, in decreasing order). After endogenous peroxidase activity was blocked with 0.3 % (v/v) hydrogen peroxide for 10 min, the sections were washed with phosphate-buffered saline (PBS) and incubated overnight with rabbit LIMK2(A5409) and p-CFL1 (AP0178) antibody at a dilution of 1:400 in a humidified chamber at 4 °C. After washing with PBS, the sections were incubated with goat against rabbit secondary antibody (IgG-HRP, 1:2000, Abcam , ab205718) for 30 min at 37 °C and then with horseradish peroxidase-labeled streptavidin for 30 min at 37 °C. Diaminobenzidine (DAB) was used as the chromogen, and the sections were subsequently counterstained with hematoxylin, dehydrated, cleared, and mounted. The quantification of IHC results was performed by using ImageJ. The average density of 5 random regions of each sample is considered the value of that sample (Leica DMI4000).

2.17. Statistical analysis

All experiments were performed at least three separate times with data obtained from triplicate wells in each experiment. The results are expressed as the means ± SEM. The significant differences between two groups were analyzed by unpaired Student's *t-test* (two-tailed); multiple groups were compared using one-way analysis of variance (Tukey post hoc test) (GraphPad Prism 8.0; GraphPad Software; GraphPad, Bethesda, MD). A value of $p < 0.05$ was considered significant.

3. Results

3.1. A549R and H1299R cells exhibited strong radioresistance

To identify the radioresistance of the cell models, single-cell gel electrophoresis (comet assay) was performed. As the data show, the DNA from the A549 and H1299 cells was damaged in an irradiation dose-dependent manner, presenting with a longer tail with 2-fold increase. However, A549R and H1299R cells had less damage with shorter tails than A549 and H1299 cells (1.3-fold increase) (Fig. 1, A-D).

Colony formation and tumor sphere formation assays were conducted to analyze the radiosensitivity of the cells at different doses. Compared with unirradiated cells, the tumor-sphere volume of parent cells (2, 4 Gy) was significantly decreased (A549 and H1299 cells showed an 0.5-fold decrease under 2 Gy and an 0.3-fold decrease under 4 Gy), while there was no obvious change in the radiation-resistant cells (A549R and H1299R cells showed an 0.96-fold decrease under 2 Gy and an 0.64- to 0.75-fold decrease under 4 Gy). The tumor spheres formed by A549R and H1299R cells were larger than those formed by A549 and H1299 cells after X-ray treatment (Fig. 1, E-H).

Compared with unirradiated cells, the colony formation of parent cells (2, 4 Gy) was significantly decreased (A549 and H1299 cells showed an 0.6-fold decrease under 2 Gy and an 0.5-fold decrease under 4 Gy), while there was no obvious change in the radiation-resistant cells (A549R and H1299R cells showed an 0.84-fold decrease under 2 Gy and an 0.75-fold decrease under 4 Gy). The colonies formed by A549R and H1299R cells were larger than those formed by A549 and H1299 cells after X-ray treatment (Fig. 1, I-L).

These results suggest that A549R and H1299R cells have stronger radioresistance than their parental lines.

3.2. NSCLC radioresistant cells had better viability and mobility

CCK8 assays were conducted to analyze cell viability. A549 and H1299 cell viability was inhibited by radiation in a dose-dependent

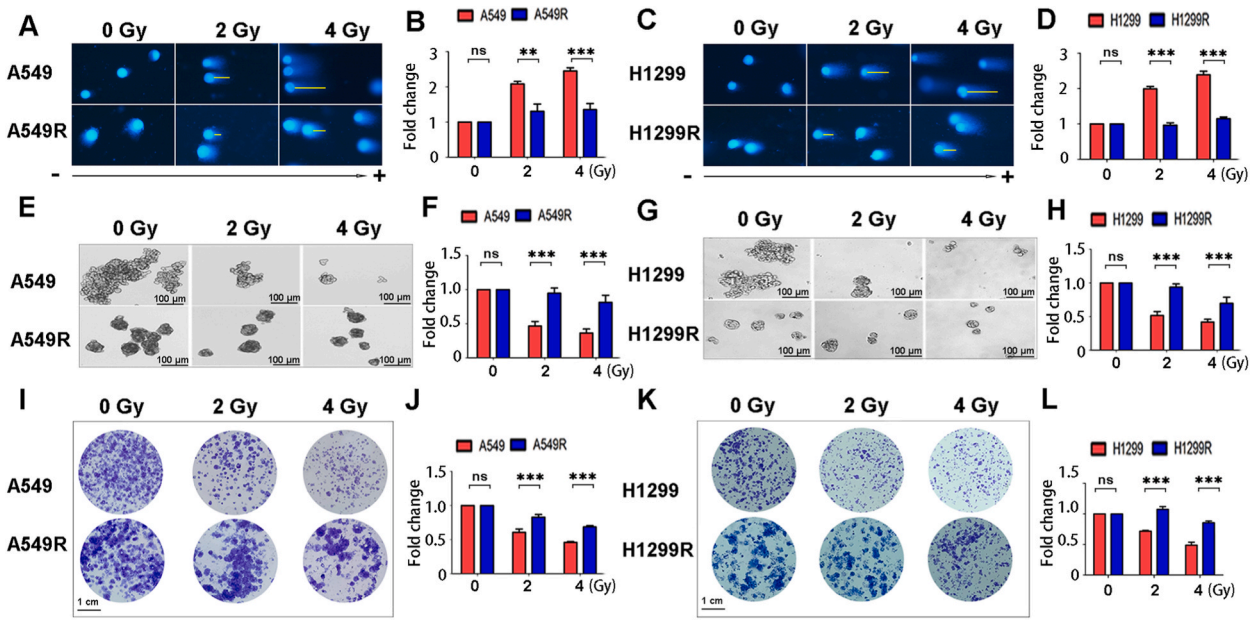

Fig. 1. A549R and H1299R cells exhibited strong radioresistance (A) Effect of RT on DNA damage (comet assay) of A549 and A549R cells. (B) Data showed as bar graph by the fold change of A549 and A549R cells tail. (C) Effect of RT on DNA damage of H1299 and H1299R cells. (D) Data showed as bar graph by the fold change of H1299 and H1299R cells tail. (E) Effect of RT on tumor sphere formation of A549 and A549R cells. (F) Data showed as bar graph by the relative value of spheres. (G) Effect of RT on tumor sphere formation of H1299 and H1299R cells. (H) Data showed as bar graph by the relative value of spheres. (I) Effect of RT on clone formation of A549 and A549R cells. (J) Data showed as bar graph by the fold change of A549 and A549R cells. (K) Effect of RT on clone formation of A549 and A549R cells. (L) Data showed as bar graph by the fold change of H1299 and H1299R cells. All experiments were repeated at least three times. (n = 3 per group, ns, P > 0.05, **P < 0.01, ***P < 0.001).

manner at every 2 days after radiation (A549 showed 80 %, 60 %, 50 % and 30 % decreases, respectively; H1299 showed 85 %, 70 %, 63 % and 41 % decreases, respectively). Compared with their parental cells, A549R and H1299R cells showed more viability after treatment with radiation (A549R cells showed 98 %, 92 %, 73 % and 60 % decreases, respectively; H1299R cells showed 98 %, 95 %, 71 % and 61 % decreases, respectively) (Fig. 2, A-B). These data suggest that low-dose irradiation significantly inhibits the growth of NSCLC parental cells. However, radiation-resistant NSCLC cells are more viable after irradiation. Based on this partial result we noticed that a decrease in the viability of radio-resistant cells at a radiation dose of 6 Gy. To ensure better comparability, we selected doses of 2 or 4 Gy in the subsequent experiment.

Their migration capacity was represented by the wound closure area. Compared with unirradiated cells, the closure areas of A549 cells were 30 % and 40 % at 48 h and 60 % and 47 % at 72 h, respectively. The closure areas of A549R cells were 83 % and 80 % at 48 h and 90 % and 85 % at 72 h, respectively (Fig. 2C–F). The closure areas of H1299 cells were 42 % and 29 % at 48 h and 63 % and 41 % at 72 h, respectively. The closure areas of H1299R cells were 59 % and 42 % at 48 h and 100 % and 60 % at 72 h (Fig. 2, G-J). Compared to the parental, untreated A549 and H1299 cells, irradiation with various doses caused a significant decrease in the closure area. A549R and H1299R cells showed faster closure rates than A549 and H1299 cells under various radiation doses. Furthermore, the radiation-resistant group showed nearly no difference in closure area compared with the nonirradiated group under 2 Gy irradiation. These data show that NSCLC radioresistance cells retain more powerful migratory abilities than their NSCLC parental cells under low-dose

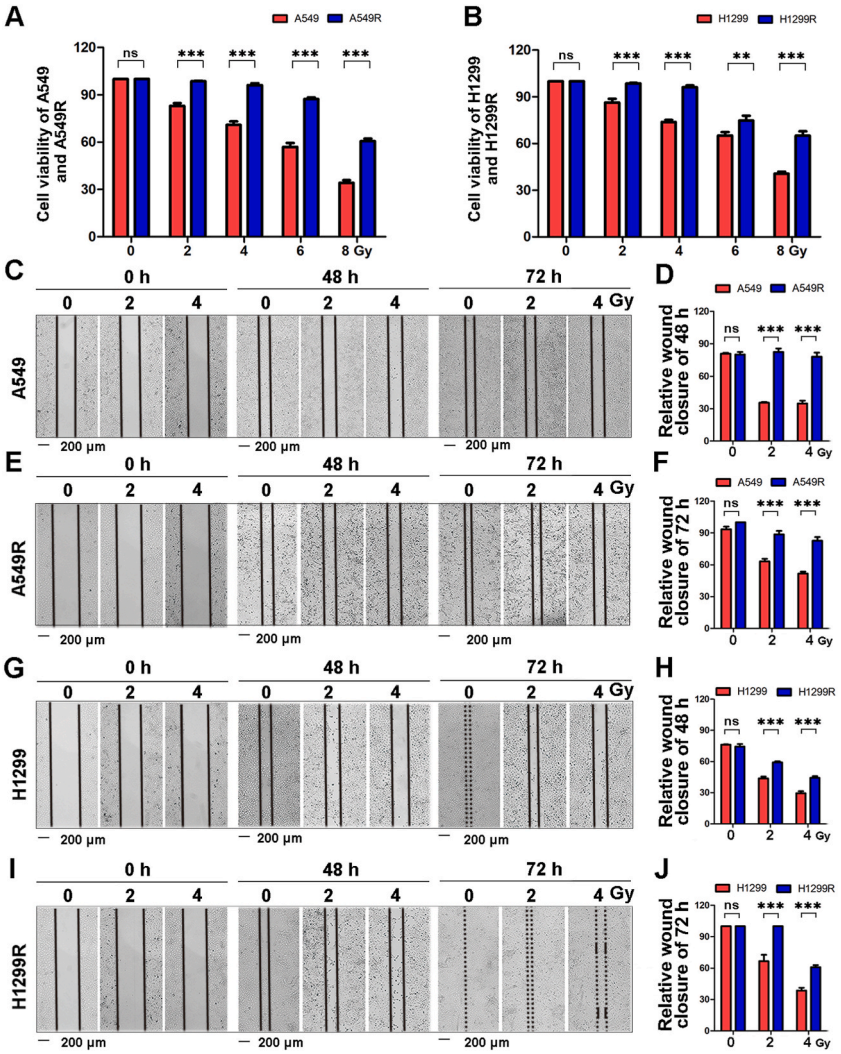

Fig. 2. NSCLC radioresistant cells possessed more activity and powerful migratory abilities (A) Effect of RT on cell viability of A549 and A549R cells was evaluated with a CCK-8 kit. (B) Effect of RT on cell viability of H1299 and H1299R cells was evaluated with a CCK-8 kit. (C) Effect of RT on cell migration of A549 cells. (D) Data showed as bar graph by the wound closure area. (E) Effect of RT on cell migration of A549R cells. (F) Data showed as bar graph by the wound closure area. (G) Effect of RT on cell migration of H1299 cells. (H) Data showed as bar graph by the wound closure area. (I) Effect of RT on cell migration of H1299R cells. (J) Data showed as bar graph by the wound closure area. All experiments were repeated at least three times. (n = 3 per group, ns, $P > 0.05$, **$P < 0.01$, ***$P < 0.001$).

irradiation. According to this partial result, we observed a significant effect of irradiation at 48 h. Thus, for the second part of the experiment, we selected this time point.

3.3. NSCLC radioresistant cells exhibited the otherness in cell adhesion molecules

To elucidate the change of gene expression of NSCLC, we firstly detected total mRNA levels between A549 and A549R cells by RNAseq. Our data showed that a huge amount of genes changed between two cell lines, including downregulation of 3488 genes and upregulation of 2273 genes (Fig. 3A). Based on inductive analysis of differential gene, we obtained KEGG pathway and GO analysis. On

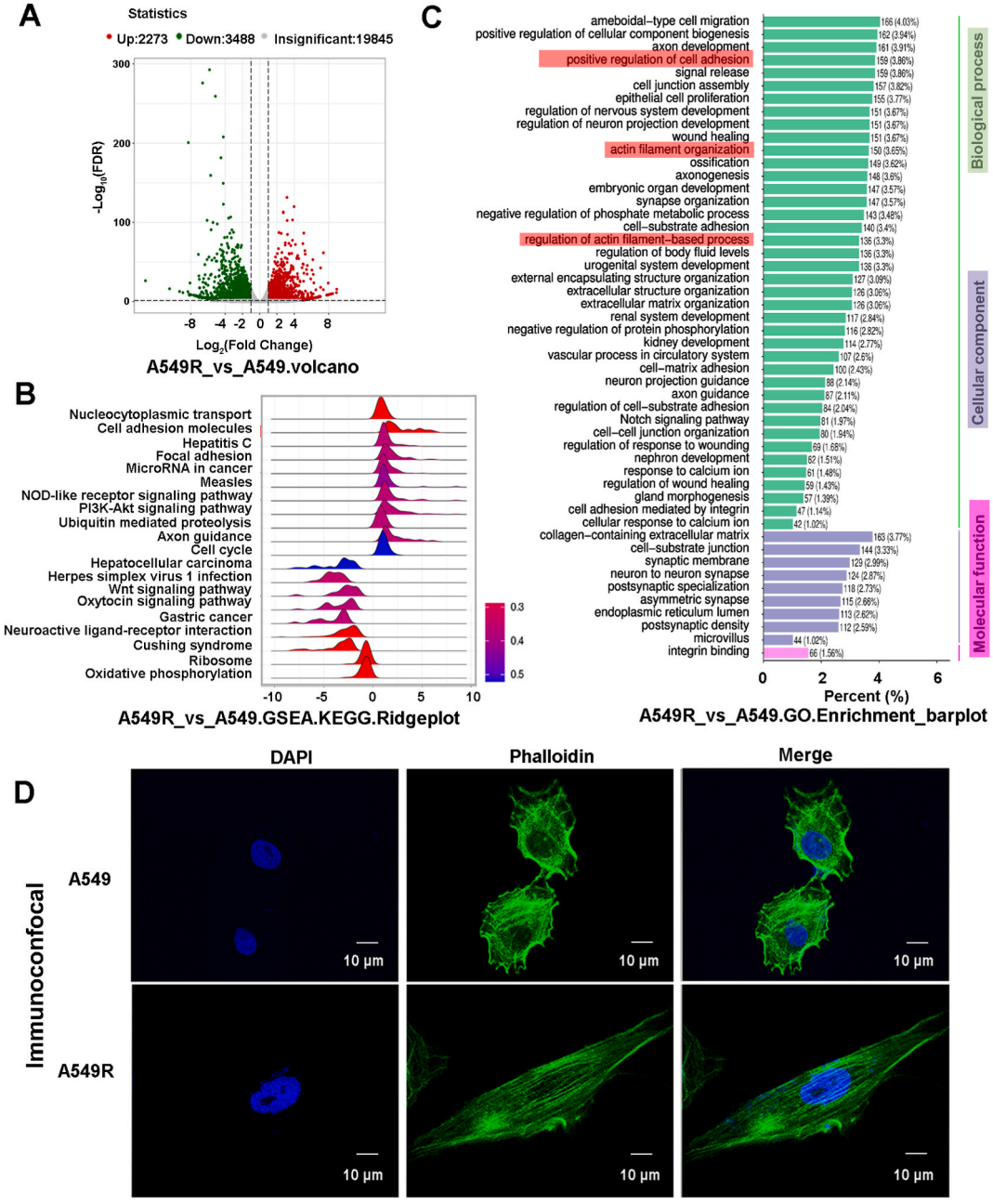

Fig. 3. NSCLC radioresistant cells exhibits the otherness in cell adhesion molecules (A) The volcano map of differentially expressed genes from A54 and A54R cells. (B) KEGG pathways which involved by differentially expressed genes. Cell adhesion molecules are marked by red rectangle. (C) GO analysis, differential GO term in biological process (BP), cellular component (CC) and Molecular Function (MF). Positive regulation of cell adhesion and regulation of action filament-based process are marked by red rectangle. (D) Cells incubated with fluorescence labeling phalloidin, and pictures of immunoconfocal to show cytoskeleton.

KEGG pathway, we found cell adhesion molecules possess a significant difference between A549 and A549R cells (Fig. 3B). Meanwhile, on GO term, we concluded positive regulation of cell adhesion and regulation of action filament-based process are discrepancy (Fig. 3C). Based on the analysis, we conducted that NSCLC radioresistant cells exhibits the otherness of cell adhesion molecules, which indicated such molecules may involve in the cells to development radioresistant. Then we used phalloidin to label F-actin for showing cytoskeleton, and we found the form of cytoskeleton are deference between A549 an A549R obviously (Fig. 3D).

3.4. The expression of apoptosis, transfer-related proteins and LIMK2 was upregulated in NSCLC radioresistance cells

The expression of anti-apoptotic protein BCL2 in A549R and H1299R cells was analyzed by western blotting. The expression of p-BCL2 was upregulated after RT (2-fold and 1.87-fold increase, respectively) (Fig. 4A–C). The expression of transfer-related proteins N-cadherin in A549R and H1299R cells was analyzed by western blotting. The expression of N-cadherin was upregulated after RT (6-fold increase) (Fig. 4D–E). According to KEGG and GO analysis, we detected the expressions of LIMK2 in A549, A549R, H1299 and H1299R cells by Western blot. As the data show, the expressions of LIMK2 were up-regulated in A549R and H1299R cells (1.8-fold and 1.6-fold increase respectively) (Fig. 4F–G). A549R and H1299R cells were treated with various radiation doses (0, 4 Gy). The expression levels of LIMK2 and p-CFL1 in A549R and H1299R cells were upregulated by irradiation (LIMK2 of A549R: 1.82-fold increase under 4 Gy. p-CFL1 of A549R: 1.74-fold increase under 4 Gy. LIMK2 of H1299R: 2.3-fold increase under 4 Gy. p-CFL1 of H1299R: 2-fold increase under 4 Gy) (Fig. 4, H-J).

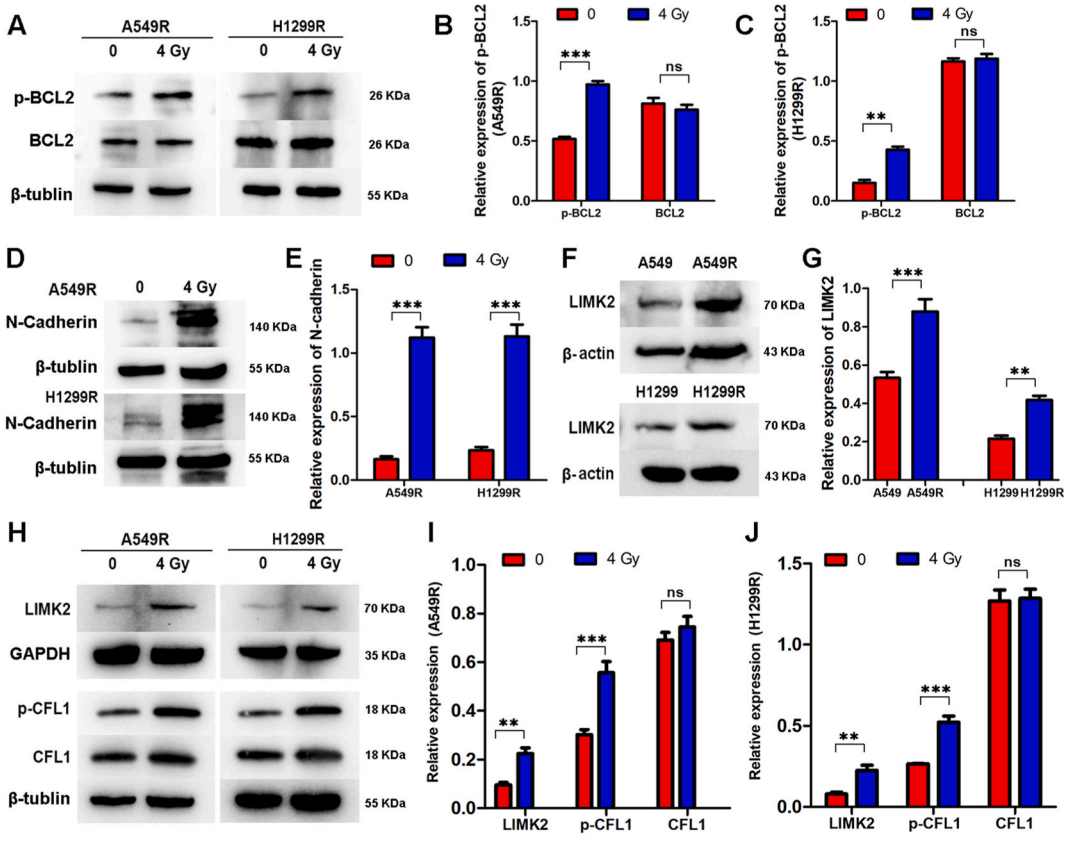

Fig. 4. Irradiation upregulates apoptosis, transfer-related proteins and LIMK2 in radiotherapy-resistant NSCLC cells (A) The expression of p-BCL2 was measured by western blotting in A549R and H1299R cells. (B) Data showed as bar graph by the relative expression of p-BCL2 in A549R cells according to gray value. (C) Data showed as bar graph by the relative expression of p-BCL2 in H1299R cells according to gray value. (D) The expression of N-cadherin was measured by western blotting in A549R and H1299R cells. (E) Data showed as bar graph by the relative expression of N-cadherin in A549R and H1299R cells according to gray value. (F) The expression of LIMK2 was measured by western blotting in A549, A549R, H1299 and H1299R cells. (G) Data showed as bar graph by the relative expression of LIMK2 in cells according to gray value. (H) The expression of LIMK2 and p-CFL1 was measured by western blotting in A549R and H1299R cells. (I) Data showed as bar graph by the relative expression of LIMK2 and p-CFL1 in A549R cells according to gray value. (J) Data showed as bar graph by the relative expression of LIMK2 and p-CFL1 in H1299R cells according to gray value. All the phosphorylation levels of proteins are the result of comparison with their total proteins. And the total protein expression levels were compared with their internal parameters. The data are presented as a representative experiment from triplicate results. ($n = 3$ per group, ns, $P > 0.05$, $^{**}P < 0.01$, $^{***}P < 0.001$).

3.5. LIMK2 was overexpressed in NSCLC radiotherapy-resistant xenografts

Given that NSCLC radioresistance cells exhibited more cell viability, migration, tumor stem cell properties and LIMK2 expression under low-dose irradiation in vitro, we next validated this effect in a mouse NSCLC xenograft model.

In the A549 group, the tumor volume of mice treated with irradiation was significantly reduced (Fig. 5, A), and the tumor tissue was destroyed compared with unirradiated controls (Fig. 5, C), while in the A549R group the tumor volume had less change (Fig. 5B). According to the TUNEL staining, apoptotic cells were more prominent in the irradiation-treated tumors than in the control tumors (Fig. 5D–F). The increase in LIMK2 protein levels were detected by IHC (Fig. 5, G-I). The A549R group showed more resistance to radiotherapy than the A549 group. The increase in p-CFL1 protein levels were detected by IHC (Fig. 5, J-L). In the A549R group, there was little change in tumor volume and less tumor tissue damage and apoptosis after irradiation than in the unirradiated control group. The increase in LIMK2 and p-CFL1protein levels was detected by IHC. These results demonstrate that 8 Gy irradiation in three consecutives radiotherapy treatments have little effect on the NSCLC radioresistance model in vivo. Moreover, the increased expression of LIMK2 in A549R relative to A549 was confirmed in vivo.

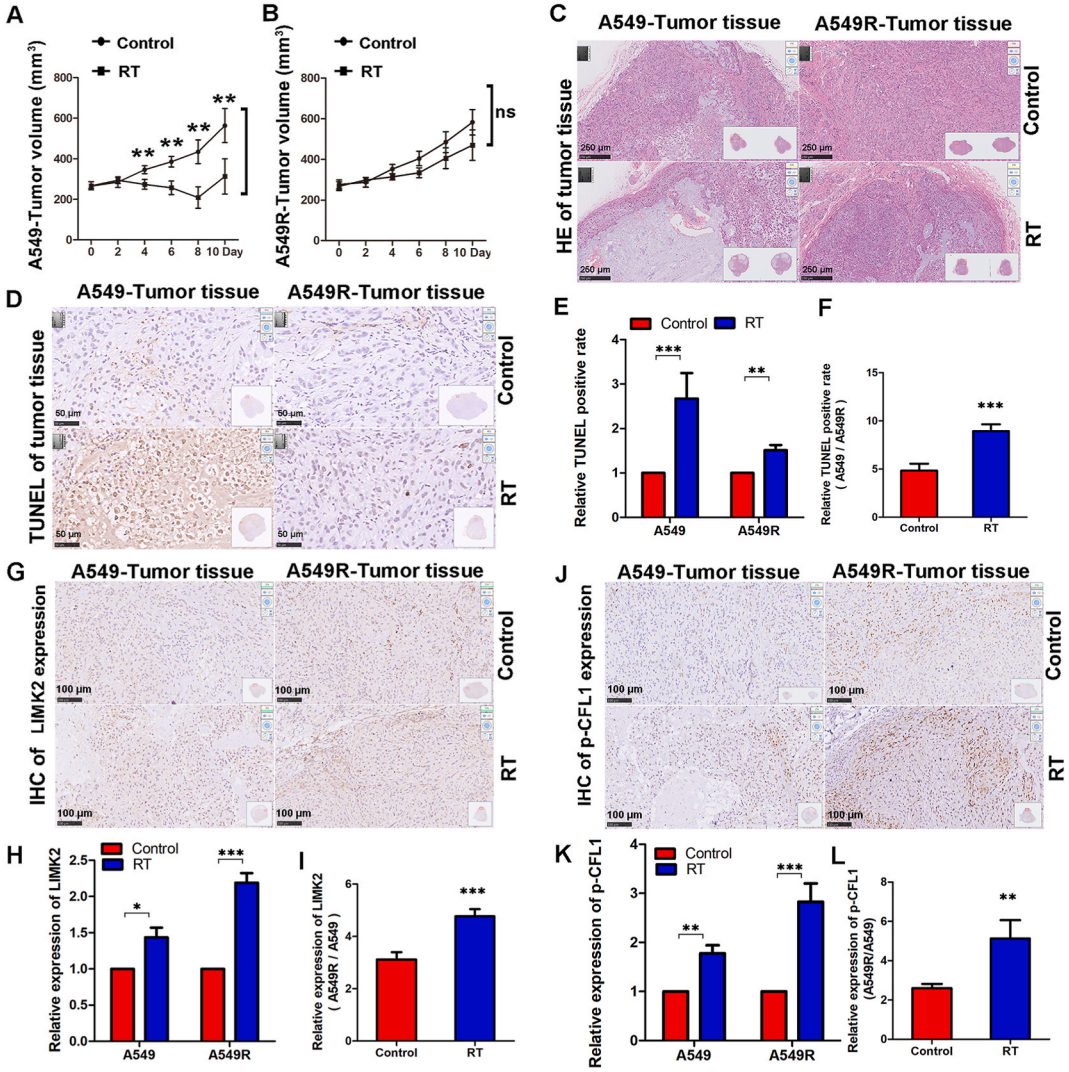

Fig. 5. LIMK2-p-CFL1 is overexpressed in radiotherapy-resistant NSCLC mice (A) The tumor volume of A549 group measured at the indicated number of days. (B) The tumor volume of A549R group measured at the indicated number of days. (C) Representative results of the HE staining of tumor sections. (D) Representative results of TUNEL staining of tumor sections. (E–F) Data showed as bar graph by relative TUNEL positive rate. (G) The expression of LIMK2 in tumor analyzed by IHC. (H–I) Data of relative LIMK2 expression showed as bar graph by relative expression positive rate. (J) The expression of p-CFL1 in tumor analyzed by IHC. (K–L) Data of relative p-CFL1 expression showed as bar graph by relative expression positive rate. (n = 5 per group, ns, $P > 0.05$, *$P < 0.05$, **$P < 0.01$, ***$P < 0.001$).

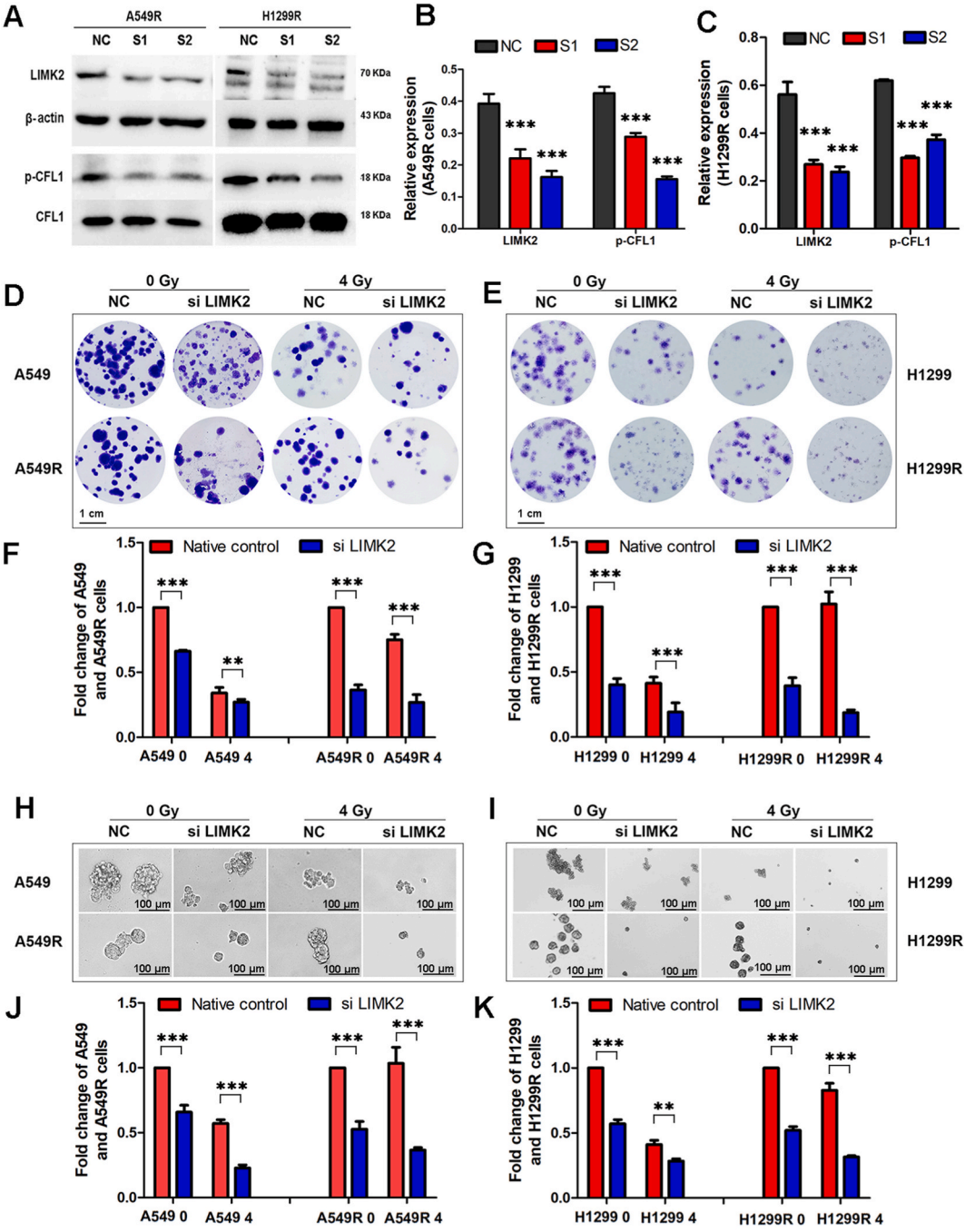

Fig. 6. Knockdown of LIMK2 expression enhances the radiotherapy sensitivity of radioresistant NSCLC cells (A) The expression of LIMK2 and p-CFL1 after LIMK2 knockdown. All the phosphorylation levels of proteins are the result of comparison with their total proteins. And the total protein expression levels were compared with their internal parameters. (B) The relative expression of LIMK2 and p-CFL1 in A549R cells according to gray value. All the phosphorylation levels of proteins are the result of comparison with their total proteins. And the total protein expression levels were compared with their internal parameters. (C) The relative expression of LIMK2 and p-CFL1 in H1299R cells according to gray value. (D) Effect of RT on clone formation of A549 and A549R cells after LIMK2 knockdown. (E) Effect of RT on clone formation of H1299 and H1299R cells after LIMK2 knockdown. (F) Data showed as bar graph by the fold change of A549 and A549R cells. (G) Data showed as bar graph by the fold change of H1299 and H1299R cells. (H) Effect of RT on tumor sphere formation of A549 and A549R cells after LIMK2 knockdown. (I) Effect of RT on tumor sphere formation of H1299 and H1299R cells after LIMK2 knockdown. (J) Data showed as bar graph by the fold change of A549 and A549R cells. (K) Data showed as bar graph by the fold change of H1299 and H1299R cells. The data are presented as a representative experiment from triplicate results. NC, negative control. (n = 3 per group, **P < 0.01, ***P < 0.001).

3.6. LIMK2 had a crucial role in radiation resistance processes

To confirm the role of LIMK2 in NSCLC radioresistant cells, si-LIMK2 was used in A549R and H1299R cells. The interference effect of si-LIMK2 is shown in Fig. 6, A-C (S1, 0.5-fold decrease, S2, 0.6- to 0.7-fold decrease). The expression of p-CFL1 was decreased simultaneously. Based on these data, S2 was used in the subsequent studies.

The effect of si-LIMK2 on A549R and H1299R cells was determined through colony formation and tumor sphere formation assays. Compared with the negative control group, colony formation was significantly decreased when LIMK2 was knocked down (A549, 0.5- to 0.7-fold decrease; A549R, 0.24- to 0.3-fold decrease; H1299, 0.5-fold decrease; H1299R, 0.3-fold decrease) (Fig. 6D–G). Tumor sphere formation was also decreased when LIMK2 was knocked down (A549, 0.5- to 0.65-fold decrease; A549R, 0.3- to 0.5-fold decrease; H1299, 0.55- to 0.7-fold decrease; H1299R, 0.5-fold decrease) (Fig. 6, H–K). These data show that LIMK2 plays an important role in radioresistance.

Our data showed that NSCLC radioresistant cells were more viable under irradiation. Compared with the negative control group, the viabilities of A549R and H1299R cells were significantly decreased in the si-LIMK2 group (50 % decrease) (Fig. 7, A-B).

The negative control group and si-LIMK2 group cells were treated with 0 or 4 Gy, and then apoptosis was detected by Annexin V staining assays. Compared with the negative control group, 4 Gy radiation induced more apoptosis when LIMK2 was knocked down in A549R and H1299R cells (Fig. 7, C-E).

We have confirmed that NSCLC radioresistance cells migrate faster than their parental cell lines. To determine the effect of LIMK2 expression on the migration of NSCLC radioresistant cells, si-LIMK2 was used before conducting cell migration experiments. The

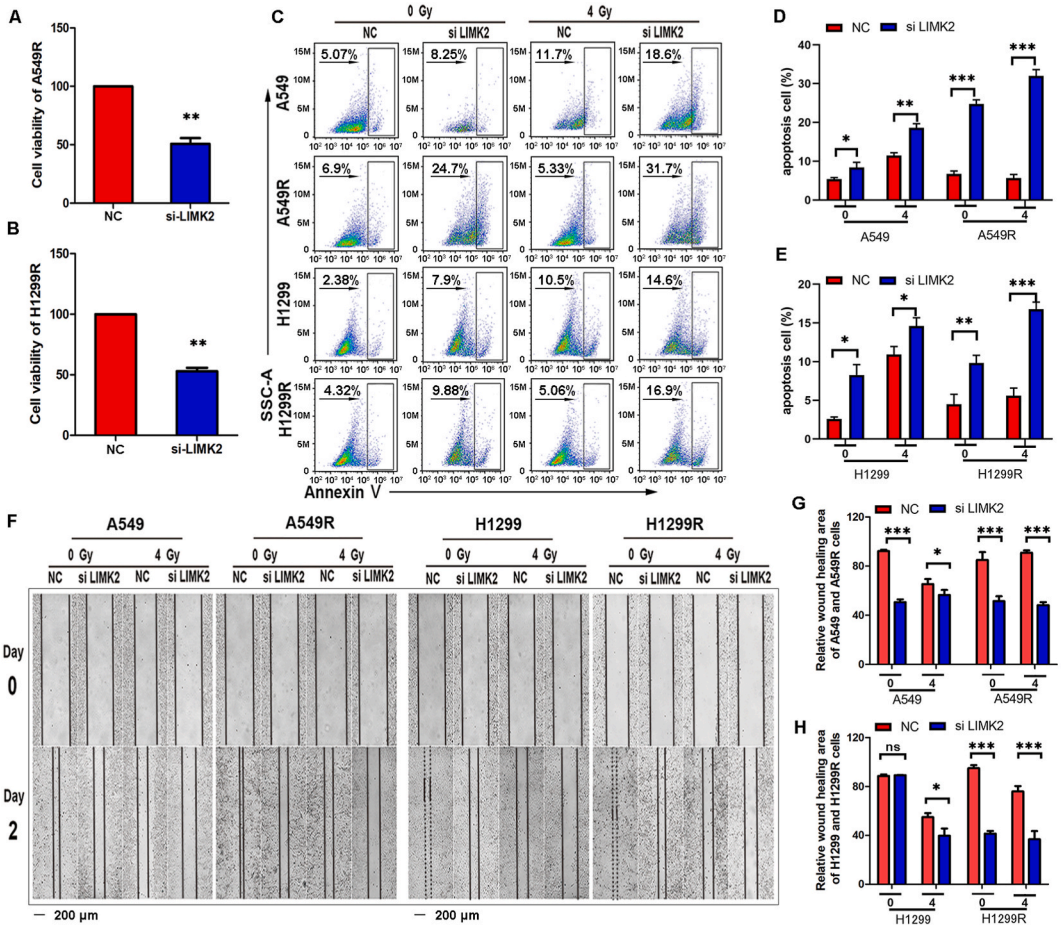

Fig. 7. Knockdown of LIMK2 expression can promote apoptosis and inhibit the viability and migration of NSCLC radioresistant cells (A) Effect of RT on cell viability of A549R cells after LIMK2 knockdown was evaluated with a CCK-8 kit. (B) Effect of RT on cell viability of H1299R cells after LIMK2 knockdown was evaluated with a CCK-8 kit. (C) Effect of RT on cells apoptosis after LIMK2 knockdown was measured with an Annexin V staining assay. Numbers within the graph denote the percentage of apoptosis. (D) Data showed as bar graph by the percentage of A549 and A549R cells. (E) Data showed as bar graph by the percentage of H1299 and H1299R cells. (F) Effect of RT on cell migration after LIMK2 knockdown was analyzed by the wound closure rate of A549, A549R, H1299 and H1299R cells. (G) Data showed as bar graph by the wound closure area of A549 and A549R cells. (H) Data showed as bar graph by the wound closure area of H1299 and H1299R cells. The data are presented as a representative experiment from triplicate results. NC, negative control. (n = 3 per group, ns, $P > 0.05$, *$P < 0.05$, **$P < 0.01$, ***$P < 0.001$).

negative control group and si-LIMK2 group cells were treated with 0 or 4 Gy, and then migration was analyzed by the wound closure rate. Compared with the negative control, the wound closure rate was slower under 4 Gy radiation when LIMK2 was knocked down (A549R, 50 % decreased; H1299R, 50 % decreased) (Fig. 7, F–H). These data show that LIMK2 plays an essential role in tumor cell migration, especially in NSCLC radioresistant cells.

4. Discussion

Radiotherapy is widely used to treat the majority of solid tumors. Radioresistance has always been one of the main obstacles to tumor treatment, leading to tumor recurrence and a reduced survival rate. Hence, how to improve the therapeutic effect of radiotherapy-resistant is a focus of research. It was reported that JAK2/STAT3/CCND2 signaling contributes to cancer stemness and radioresistance [21]. Otherwise, UBE2T-mediated H2AX/γH2AX monoubiquitination on facilitating cell cycle arrest activation to cuase radiation-induced DNA repair, which conferring hepatocellular carcinoma radioresistance [22]. In triple-negative breast cancer, THOC-mediated transnuclear export of pluripotency transcripts plays a critical role in promoting cancer stemness and contributing to radioresistance [23]. Nevertheless, we focused on the regulation of cell skeletal protein in NSCLC radioresistance.

In this work, our data demonstrate a critical role of LIMK2 in mediating NSCLC resistance to radiotherapy and show that knockdown of LIMK2 expression may be an important target for reversing radiotherapy resistance in NSCLC.

The most important function of LIMK2 is the regulation of cell skeletal proteins, which are involved in cell growth, migration, epithelial-mesenchymal transition (EMT) and other biological functions. Interestingly, we observed that the cell morphology of A549R and H1299R cells was significantly different from that of their parental cell lines (A549, H1299) (data not shown). It is well known that cell morphology is closely related to cytoskeleton proteins. LIM-domain containing kinase 1 and 2 (LIMK1 and LIMK2) are a family of serine/threonine protein kinases. Whether LIMK1 and LIMK2, as an important kinase regulating skeletal proteins, is involved in radiotherapy resistance in NSCLC remains poorly characterized. In our preliminary experiment, both LIMK1 and LIMK2 were detected, but there was no significant difference observed in LIMK1 (data not shown).

To reveal the effect of irradiation on NSCLC radioresistance cells and NSCLC parental cells, we detected cell viability and DNA damage. The data showed that A549 and H1299 cell viability was inhibited by radiation in a dose-dependent manner (Fig. 2A and B). However, radiation had little effect on A549R and H1299R cells. Meanwhile, we found that the DNA of A549 and H1299 cells was damaged in an irradiation dose-dependent manner and presented with a longer tail in comet assays (Fig. 1A–D). A549R and H1299R cells had less DNA damage with shorter tails under 4 Gy irradiation. Moreover, NSCLC radioresistance cells also showed a faster wound closure rate (Fig. 2C–J) and more colony formation than NSCLC parental cells under low-dose irradiation (Fig. 1I-L). Taken together, these results suggest that NSCLC radioresistance cells are more viable, invasive and malignant under low-dose irradiation in vitro and in vivo. In our previous experiment exploring radiation dose, we irradiated the parent and resistant strains with doses of 0, 2, 4, 6, and 8 Gy, respectively [24]. The results indicated that 2Gy had an inhibitory effect, while 4Gy had a significant effect on the parent cells but did not show an inhibitory effect on the resistant strains. Additionally, 6Gy showed a slight inhibitory effect on the resistant cells. Based on these findings, a dose of 4Gy was selected for the subsequent experiment.

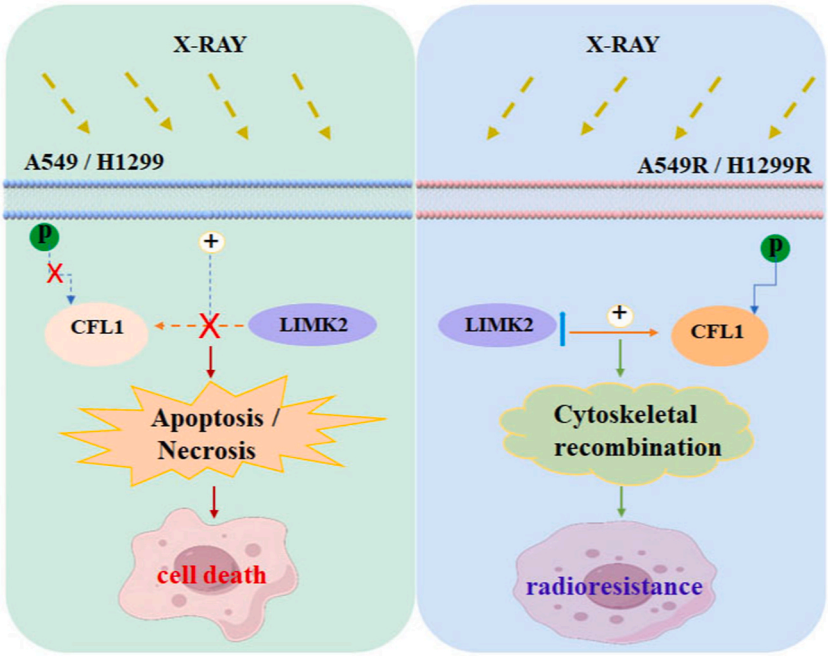

Fig. 8. LIKM2/CFL1 pathway promote the radioresistant of NSCLC cells.

We next analyzed the related molecular mechanisms of NSCLC radioresistance cells. We firstly detected total mRNA levels between A549 and A549R cells by RNAseq, which indicated cell adhesion molecules may involve in the cells to development radioresistant (Fig. 3A–C). Considering the role of LIMK2 in cellular biological processes, we found that the expression of LIMK2 was upregulated in radioresistance cells (Fig. 4F). LIMK2 is a serine/threonine/tyrosine kinase that regulates actin dynamics and subsequently causes filament organization and stress fiber formation [25]. It has been reported that LIMK2 is associated with stem cell proliferation in colorectal cancer [26], proliferation of bladder smooth muscle [27], castration resistance in prostate cancer, and metastatic progression in triple-negative breast cancer [28]. LIMK2 mediates cancer metastasis, migration, angiogenesis and invasion by phosphorylating cofilin (CFL).

Accordingly, in this study, we detected the expression of LIMK2 and p-CFL1/CFL1. First, we found that the expression of LIMK2 was upregulated in NSCLC radioresistance cells (A549R and H1299R). After irradiation (0, 4 Gy) of A549R and H1299R cells, the expression of LIMK2 and p-CFL1 was increased, while the expression of total CFL1 was not affected (Fig. 4H). Subsequently, to determine whether the LIMK2-CFL1 axis is required for NSCLC radioresistance, we knocked down LIMK2 by siRNA. Importantly, radiosensitivity to 4 Gy irradiation was enhanced by the downregulation of LIMK2 in NSCLC radioresistance cells.

In summary, we can conclude that NSCLC radioresistance cells are more viable, invasive and malignant, which could mostly mediate by the LIMK2-CFL1 axis under low-dose irradiation.

An important finding of this study is that these effects were observed in vitro and in vivo. We observed that the growth of NSCLC xenografts in mice could be inhibited by treatment with irradiation (8 Gy irradiation was administered for three consecutive days) (Fig. 5A). However, the same treatment had little effect on the growth of NSCLC radioresistance cell xenografts in mice (Fig. 5B). In addition, the upregulation of LIMK2 and p-CFL1 protein levels were observed in these xenografts (Fig. 5G, J).

In general, we systematically compared and described the differences in cell activity and migration between radiotherapy-resistant and nonresistant NSCLC cells under low-dose irradiation. In addition, we revealed a novel mechanism by which the LIMK2-CFL1 pathway manages radiotherapy resistance in NSCLC cells (Fig. 8). These results may provide a novel therapeutic strategy for attenuating NSCLC radioresistance.

Limitations of our study include not investigating the therapeutic effect of knocking down LIMK2 in a mouse model and not investigating the differences in LIMK2 expression between patients who are sensitive to radiotherapy and those who are resistant to radiotherapy. It could be important to confirm that LIMK2 promotes radiotherapy sensitivity. This will be the target of our next project.

In this study, in addition to systematically described the differences in biological characteristics between NSCLC-resistant and NSCLC-nonresistant cells under low-dose irradiation, it is more important to first observed and demonstrated the role of enzymes involved in regulating cytoskeletal proteins in radiotherapy resistance in non-small cell lung cancer. LIMK2 as having a major role in the radioresistance of NSCLC cells, which provides a theoretical basis for blocking NSCLC radiotherapy resistance.

Data availability statement

The raw data cannot be shared temporarily because it also forms a part of another study.

Ethics statement

All of the animal experiments were performed under the guidelines of Hubei University of Medicine animal use regulations and approved by the institutional animal care and use committee (IACUC) at the Hubei University of Medicine.

Funding statement

This work was supported by the Natural Science Foundation of Hubei Province of China (Nos. 2022CFB082), Natural Science Foundation of Hubei Provincial Department of Education (Nos. D20212101), the Central Government Guides Local Scientific and Technological Development project (Nos. 2022BGE270)The Foundation for Free Exploration of Hubei University of Medicine (Nos. FDFR201802), the Scientific and Technological Project of Shiyan City of Hubei Province (Nos. 21Y18), Immunoradiotherapy research fund project of Chinese Medical Association Radiation Oncology Branch (Nos. Z-2017-24-2108). Advantages Discipline Group (Medicine) Project in Higher Education of Hubei Province (2021–2025, Nos. 2022XKQT2).

Patient consent for publication

Not applicable.

CRediT authorship contribution statement

Chao Tian: Data curation. **Zhen Peng:** Data curation. **Lei Chang:** Writing – review & editing, Writing – original draft, Methodology. **Xinzhou Deng:** Writing – original draft. **Shan Jiang:** Data curation. **Jiahui Han:** Data curation. **Can Ye:** Formal analysis. **Yutao Yan:** Writing – original draft, Supervision, Project administration, Methodology. **Zhiguo Luo:** Supervision, Project administration.

Declaration of competing interest

The authors declare that they have no known competing financial interests or personal relationships that could have appeared to influence the work reported in this paper.

Acknowledgements

We would like to thank my colleague, supervisory technician, Renhuang Sun, at the Radiotherapy Center for their help in this work.

References

[1] H. Sung, J. Ferlay, R.L. Siegel, M. Laversanne, I. Soerjomataram, A. Jemal, F. Bray, Global cancer statistics 2020: GLOBOCAN estimates of incidence and mortality worldwide for 36 cancers in 185 countries, CA Cancer J Clin 71 (2021) 209–249, https://doi.org/10.3322/caac.21660.
[2] S.C. Formenti, N.P. Rudqvist, E. Golden, B. Cooper, E. Wennerberg, C. Lhuillier, C. Vanpouille-Box, K. Friedman, L. Ferrari de Andrade, K.W. Wucherpfennig, A. Heguy, N. Imai, S. Gnjatic, R.O. Emerson, X.K. Zhou, T. Zhang, A. Chachoua, S. Demaria, Radiotherapy induces responses of lung cancer to CTLA-4 blockade, Nat. Med. 24 (2018) 1845–1851, https://doi.org/10.1038/s41591-018-0232-2.
[3] M.S. Binkley, Y.J. Jeon, M. Nesselbush, E.J. Moding, B.Y. Nabet, D. Almanza, C. Kunder, H. Stehr, C.H. Yoo, S. Rhee, M. Xiang, J.J. Chabon, E. Hamilton, D. M. Kurtz, L. Gojenola, S.G. Owen, R.B. Ko, J.H. Shin, P.G. Maxim, N.S. Lui, L.M. Backhus, M.F. Berry, J.B. Shrager, K.J. Ramchandran, S.K. Padda, M. Das, J. W. Neal, H.A. Wakelee, A.A. Alizadeh, B.W. Loo Jr., M. Diehn, KEAP1/NFE2L2 mutations predict lung cancer radiation resistance that can Be targeted by glutaminase inhibition, Cancer Discov. 10 (2020) 1826–1841, https://doi.org/10.1158/2159-8290.cd-20-0282.
[4] K. Wang, J.E. Tepper, Radiation therapy-associated toxicity: etiology, management, and prevention, CA Cancer J Clin 71 (2021) 437–454, https://doi.org/10.3322/caac.21689.
[5] D.J. Craig, N.S. Nanavaty, M. Devanaboyina, L. Stanbery, D. Hamouda, G. Edelman, L. Dworkin, J.J. Nemunaitis, The abscopal effect of radiation therapy, Future Oncol. 17 (2021) 1683–1694, https://doi.org/10.2217/fon-2020-0994.
[6] Z. Li, Y. Zhang, S. Sui, Y. Hua, A. Zhao, X. Tian, R. Wang, W. Guo, W. Yu, K. Zou, W. Deng, L. He, L. Zou, Targeting HMGB3/hTERT axis for radioresistance in cervical cancer, J. Exp. Clin. Cancer Res. 39 (2020) 243, https://doi.org/10.1186/s13046-020-01737-1.
[7] J. Ma, J.A. Benitez, J. Li, S. Miki, C. Ponte de Albuquerque, T. Galatro, L. Orellana, C. Zanca, R. Reed, A. Boyer, T. Koga, N.M. Varki, T.R. Fenton, S.K. Nagahashi Marie, E. Lindahl, T.C. Gahman, A.K. Shiau, H. Zhou, J. DeGroot, E.P. Sulman, W.K. Cavenee, R.D. Kolodner, C.C. Chen, F.B. Furnari, Inhibition of nuclear PTEN tyrosine phosphorylation enhances glioma radiation sensitivity through attenuated DNA repair, Cancer Cell 36 (2019) 690–691, https://doi.org/10.1016/j.ccell.2019.11.008.
[8] Q. Liu, Y. Hao, R. Du, D. Hu, J. Xie, J. Zhang, G. Deng, N. Liang, T. Tian, L. Kasmann, D. Rades, C.H. Rim, P. Hu, J. Zhang, Radiotherapy programs neutrophils to an antitumor phenotype by inducing mesenchymal-epithelial transition, Transl. Lung Cancer Res. 10 (2021) 1424–1443, https://doi.org/10.21037/tlcr-21-152.
[9] J. Port, N. Muthalagu, M. Raja, F. Ceteci, T. Monteverde, B. Kruspig, A. Hedley, G. Kalna, S. Lilla, L. Neilson, M. Brucoli, K. Gyuraszova, J. Tait-Mulder, M. Mezna, S. Svambaryte, A. Bryson, D. Sumpton, A. McVie, C. Nixon, M. Drysdale, H. Esumi, G.I. Murray, O.J. Sansom, S.R. Zanivan, D.J. Murphy, Colorectal tumors require NUAK1 for protection from oxidative stress, Cancer Discov. 8 (2018) 632–647, https://doi.org/10.1158/2159-8290.cd-17-0533.
[10] J.M. Noh, S.C. Choi, M.H. Song, K.S. Kim, S. Jun, J.H. Park, J.H. Kim, K. Kim, T.H. Ko, J.I. Choi, J.A. Gim, J.H. Kim, Y. Jang, Y. Park, J.E. Na, I.J. Rhyu, D.S. Lim, The activation of the LIMK/cofilin signaling pathway via extracellular matrix-integrin interactions is critical for the generation of mature and vascularized cardiac organoids, Cells (2023) 12, https://doi.org/10.3390/cells12162029.
[11] Y. Niu, F. Ma, W. Huang, S. Fang, M. Li, T. Wei, L. Guo, Long non-coding RNA TUG1 is involved in cell growth and chemoresistance of small cell lung cancer by regulating LIMK2b via EZH2, Mol. Cancer 16 (2017) 5, https://doi.org/10.1186/s12943-016-0575-6.
[12] K. Nikhil, L. Chang, K. Viccaro, M. Jacobsen, C. McGuire, S.R. Satapathy, M. Tandiary, M.M. Broman, G. Cresswell, Y.J. He, G.E. Sandusky, T.L. Ratliff, D. Chowdhury, K. Shah, Identification of LIMK2 as a therapeutic target in castration resistant prostate cancer, Cancer Lett. 448 (2019) 182–196, https://doi.org/10.1016/j.canlet.2019.01.035.
[13] D.R. Croft, D. Crighton, M.S. Samuel, F.C. Lourenco, J. Munro, J. Wood, K. Bensaad, K.H. Vousden, O.J. Sansom, K.M. Ryan, M.F. Olson, p53-mediated transcriptional regulation and activation of the actin cytoskeleton regulatory RhoC to LIMK2 signaling pathway promotes cell survival, Cell Res. 21 (2011) 666–682, https://doi.org/10.1038/cr.2010.154.
[14] Y. Wu, Y. Zhou, H. Gao, Y. Wang, Q. Cheng, S. Jian, Q. Ding, W. Gu, Y. Yao, J. Ma, W. Wu, Y. Li, X. Tong, X. Song, S. Ma, LYAR promotes colorectal cancer progression by upregulating FSCN1 expression and fatty acid metabolism, Oxid. Med. Cell. Longev. 2021 (2021), 9979707, https://doi.org/10.1155/2021/9979707.
[15] W. Wang, C. Yang, H. Nie, X. Qiu, L. Zhang, Y. Xiao, W. Zhou, Q. Zeng, X. Zhang, Y. Wu, J. Liu, M. Ying, LIMK2 acts as an oncogene in bladder cancer and its functional SNP in the microRNA-135a binding site affects bladder cancer risk, Int. J. Cancer 144 (2019) 1345–1355.
[16] N.A. Franken, H.M. Rodermond, J. Stap, J. Haveman, C. van Bree, Clonogenic assay of cells in vitro, Nat. Protoc. 1 (2006) 2315–2319, https://doi.org/10.1038/nprot.2006.339.
[17] W. Huang, L. Zhang, M. Yang, X. Wu, X. Wang, W. Huang, L. Yuan, H. Pan, Y. Wang, Z. Wang, Y. Wu, J. Huang, H. Liang, S. Li, L. Liao, L. Liu, J. Guan, Cancer-associated fibroblasts promote the survival of irradiated nasopharyngeal carcinoma cells via the NF-kappaB pathway, J. Exp. Clin. Cancer Res. 40 (2021) 87, https://doi.org/10.1186/s13046-021-01878-x.
[18] D.E. Pefani, R. Latusek, I. Pires, A.M. Grawenda, K.S. Yee, G. Hamilton, L. van der Weyden, F. Esashi, E.M. Hammond, E. O'Neill, RASSF1A-LATS1 signalling stabilizes replication forks by restricting CDK2-mediated phosphorylation of BRCA2, Nat. Cell Biol. 17 (2015) 531, https://doi.org/10.1038/ncb3035.
[19] C.R. Justus, N. Leffler, M. Ruiz-Echevarria, L.V. Yang, In vitro cell migration and invasion assays, J. Vis. Exp. (2014), https://doi.org/10.3791/51046.
[20] S. Johnson, H. Chen, P.K. Lo, In vitro tumorsphere formation assays, Bio Protoc 3 (2013), https://doi.org/10.21769/bioprotoc.325.
[21] S.Y. Park, C.J. Lee, J.H. Choi, J.H. Kim, J.W. Kim, J.Y. Kim, J.S. Nam, The JAK2/STAT3/CCND2 Axis promotes colorectal Cancer stem cell persistence and radioresistance, J. Exp. Clin. Cancer Res. 38 (2019) 399, https://doi.org/10.1186/s13046-019-1405-7.
[22] J. Sun, Z. Zhu, W. Li, M. Shen, C. Cao, Q. Sun, Z. Guo, L. Liu, D. Wu, UBE2T-regulated H2AX monoubiquitination induces hepatocellular carcinoma radioresistance by facilitating CHK1 activation, J. Exp. Clin. Cancer Res. 39 (2020) 222, https://doi.org/10.1186/s13046-020-01734-4.
[23] X. Bai, J. Ni, J. Beretov, S. Wang, X. Dong, P. Graham, Y. Li, THOC2 and THOC5 regulate stemness and radioresistance in triple-negative breast cancer, Adv. Sci. 8 (2021), e2102658, https://doi.org/10.1002/advs.202102658.
[24] R. Sun, C. Chen, X. Deng, F. Wang, S. Song, Q. Cai, J. Wang, T. Zhang, M. Shi, Q. Ke, Z. Luo, IL-11 mediates the radioresistance of cervical cancer cells via the PI3K/akt signaling pathway, J. Cancer 12 (2021) 4638–4647, https://doi.org/10.7150/jca.56185.
[25] O. Bernard, Lim kinases, regulators of actin dynamics, Int. J. Biochem. Cell Biol. 39 (2007) 1071–1076, https://doi.org/10.1016/j.biocel.2006.11.011.
[26] F.C. Lourenco, J. Munro, J. Brown, J. Cordero, R. Stefanatos, K. Strathdee, C. Orange, S.M. Feller, O.J. Sansom, M. Vidal, G.I. Murray, M.F. Olson, Reduced LIMK2 expression in colorectal cancer reflects its role in limiting stem cell proliferation, Gut 63 (2014) 480–493, https://doi.org/10.1136/gutjnl-2012-303883.
[27] Q. Yu, C. Wu, Y. Chen, B. Li, R. Wang, R. Huang, X. Li, D. Gu, X. Wang, X. Duan, S. Li, Y. Liu, W. Wu, M. Hennenberg, G. Zeng, Inhibition of LIM kinase reduces contraction and proliferation in bladder smooth muscle, Acta Pharm. Sin. B 11 (2021) 1914–1930, https://doi.org/10.1016/j.apsb.2021.01.005.
[28] P. Malvi, R. Janostiak, S. Chava, P. Manrai, E. Yoon, K. Singh, M. Harigopal, R. Gupta, N. Wajapeyee, LIMK2 promotes the metastatic progression of triple-negative breast cancer by activating SRPK1, Oncogenesis 9 (2020) 77, https://doi.org/10.1038/s41389-020-00263-1.